1

Optical Fiber Interferometers and Their Applications

Ali Reza Bahrampour, Sara Tofighi, Marzieh Bathaee and Farnaz Farman
Sharif University of Technology
Iran

1. Introduction

Interference as a wave characteristic of the electromagnetic wave has many applications in science, technology and medicine (Grattan & Meggit, 1997; Wang et al., 2011). The fringe visibility of the first order interference experiments such as the famous double slit Young experiment and Michelson interferometer, is determined by the first order correlation function (Gerry & Knight, 2005). The first order interference is also called the field interference. In Hanbury-Brown and Twiss (HBT) experiment, fringes are due to the intensity interference and visibility is determined by the second order correlation function. (Brown & Twiss, 1956; Scully & Zubairy 2001). In quantum optics, nonlinear Lithography and quantum Lithography, interferometry based on higher order correlation function is of prime importance (Bentley & Boyd, 2004; Boto et al., 2000). However in all of these interferometries, the fringe pattern depends on the optical path difference (OPD) and feature of light source. This chapter is concentrated on the classical field interferometry. The fringe existence is a characteristic of spatial or temporal coherences between the two light beams.

The phenomenon of interference of light is used in many high precision measuring systems and sensors. The optical path can be controlled by optical waveguides and optical fibers. The use of optical fibers allows making such devices extremely compact and economic.

Among the lots of advantages of optical fibers is their ability to reduce the effects of wave front distortion by the atmospheric turbulence and compact beam-splitter and combiner. These abilities made optical fiber as a suitable medium for transportation of light in long baseline interferometers which are used for gravitational wave detection, intruder sensor, structural health monitoring and long length leak detection systems (Sacharov, 2001; Cahill, 2007; Cahill & Stokes, 2008; Jia et al., 2008; Mishra & Soni, 2011, Bahrampour et al., 2012).

Other advantages that make optical fibers become useful elements in sensing technologies are high elongation sensitivity, fast response to internal or external defects such as temperature and tension, electromagnetic noise disturbance immunity, less power consumption and potential for large scale multiplexing (Higuera & Miguel, 2002).

In this chapter the different structures of optical fibers which are important in fiber interferometry are taken into consideration. The structures of different types of fiber interferometers are described. The sensitivity of coherent light optical fiber interferometers is compared with those of the incoherent and white light optical fiber interferometers. The

standard methods for signal recovering are explained. A brief discussion on the noise sources appears in this chapter. Due to the immunity of the optical fibers to the lightening and electromagnetic noise, optical fibers are suitable sensors for transient measurement in harsh environments such as current measurement in high voltage transformers (Grattan & Meggit, 1999). The optical fiber hydrophone systems are based on elasto-optic effect in optical fiber coil, which is installed in one arm of an optical fiber interferometer (OFI) (Freitas, 2011). The optical fiber interferometers can be employed as biochemical sensors (Gopel et al., 1991). The cooperation of optical fiber interferometry and Plasmon can improve the sensitivity of biosensors to one molecule detection system (De Vos et al., 2009). The mechanical quantities such as pressure, velocity, acceleration and displacement can be measured by optical fiber interferometers (Shizhuo et al., 2008). Among a lot of applications of optical fiber interferometers, only some applications such as linear and nonlinear photonic circuits and distributed optical fiber sensors are mentioned in this chapter.

2. Optical fibers structures

2.1 Standard fibers

An optical fiber is a cylindrical structure that transports electromagnetic waves in the infrared or visible bands of electromagnetic spectrum. In practice optical fibers are highly flexible and transparent dielectric material. The optical fiber consists of three different layers. Core is the central region which is surrounded by the cladding. These two layers are protected by protective jacket. The core refractive index can be uniform or graded while the cladding index is typically uniform. For light guiding, it is necessary that the core index be greater than the cladding index. Most of the light energy propagates in the core and only a small fraction travels in the cladding. The cladding radius is so large that the jacket has no effect on the light propagation in the optical fiber structure.

Depending on the dimensionless frequency $v = 2\pi a(n_{co}^2 - n_{cl}^2)^{1/2}/\lambda$ where a is the core radius, λ is the wavelength of the light in free space, n_{co} and n_{clad} are the core and clad refractive indices respectively, optical fibers are divided into multimode ($v \gg 1$) and single mode fibers ($0 < v < v_c$), where v_c is cutoff frequency (Agrawal, 2007).

The optical fibers whose core and cladding have very nearly the same refractive index are named weakly guiding fibers. The corresponding eigen value equation is simpler than the exact fiber characteristic equation. The notation $LP_{v,\mu}$ introduces the weakly guiding modes. The fundamental mode $HE_{1,1}$is denoted by $LP_{0,1}$(Okamoto, 2006). The normalized propagation constant versus the dimensionless frequency is called the dispersion curve.

Depending on the coupling and optical fiber physical parameters, bounded, radiation and evanescent modes can exist in an optical fiber. The total incident power can be transported by the bounded and radiation modes while evanescent modes store power near the excitation source (Snyder, 1983).

2.2 Polarization maintained optical fibers

Birefringent optical fibers are those fibers that display two distinct refractive indices depending on the polarization direction of the light entering into them. The two principal axes of the birefringent fibers are named the fast and slow axis. For a light beam whose

polarization aligned with one of the principal axes of the birefrigent fiber, the light propagates without any disturbance in its polarization state. The birefringence parameter of the fiber is defined by the difference between the two refractive indices corresponding to the two principal axes $B = n_s - n_f$, where n_s and n_f are the refractive indices of the slow and fast axis respectively. Sometimes birefringence is defined in terms of the fiber beat length $L_B = \lambda/B$ that is defined as the length of fiber over which the phase difference between the fast and slow waves becomes 2π. The beat length should be smaller than the perturbation periods introduced in the drawing process as well as the physical bends and twists. Consequently short beat length fibers preserve the polarization direction. This kind of fibers are called Polarization Maintained optical Fibers and denoted by PMF. Several types of PMFs are shown in Fig. 1 (Okamoto, 2006).

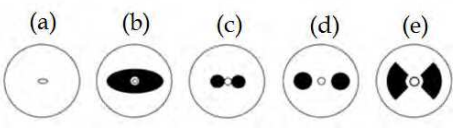

Fig. 1. Cross section of (a) elliptical core fiber (b) elliptical jacket fiber (c) side tunnel fiber (d) PANDA fiber (e) Bow-tie fiber.

2.3 Photonic crystal fibers

Light propagation in standard optical fibers and PMFs is based on the total internal reflection effect. Bragg diffraction effect can also be employed to confine the light in the core of fiber with periodic structure in the cladding. The micro structured fiber which is also called photonic crystal fiber (PCF) as shown in Fig. 2, consists of numerous air holes within a silica host. Usually the air holes are in a periodic arrangement around silica or a hollow core. The silica core PCF is called holey fiber, high delta or cobweb fiber while hollow core is named photonic band gap fiber (PBGF). The simplest structure of the holey fiber is a regular hexagonal lattice of small holes with a defect in the center such that the hole in the center is missed. In the holey fibers, guiding mechanism is also based on the total internal reflection. Air holes in the cladding area cause an effective lowering of the average refractive index (Poli, et al., 2007). In hollow-core fibers, field confinement in the air core is based on the band gap effect.

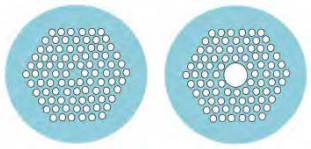

Fig. 2. Cross section of holey fiber (left) and hollow fiber (right).

2.4 Slab optical waveguide

Optical fibers are suitable transmission lines for several applications such as high capacity long-haul communication networks and long length optical interferometry. In many applications such as integrated circuits, the transmission length is less than one millimeter.

Optical waveguides are proper for such applications. A dielectric waveguide consists of a dielectric with refractive index n_1 which is deposited on a substrate with refractive index n_2. The refractive index of the medium above the layer n_1 is indicated by n_3. To achieve true guiding modes, it is necessary that n_1 be larger than n_2 and n_3. The propagating modes of the slab waveguides are TE and TM modes. The mathematical mode analysis of slab waveguides can be found in any standard text book (Adams, 1981). Depending on the propagation constant β, modes of narrow dielectric strip waveguide are also classified into the bounded, radiation and evanescent modes (Adams, 1981; Snyder, 1983).

2.5 Fiber Bragg gratings

The modes of optical fibers and waveguides are propagated without coupling to each other in the absence of any perturbation. Coupling to the desired modes can be controlled by changing the amplitude and the phase of the perturbation in the optical fiber. The coupled mode theory (CMT) can be found in the standard text books (Huang, 1984). If the refractive index of the core varies periodically, due to the Bragg diffraction effect, scattering from different periods can be constructive for some frequencies and destructive for the other ones. Depending on the period length, the periodic structures are classified as either long period grating (LPG) or fiber Bragg grating (FBG). The period of the LPG is of the order of micrometer while in the FBG, it is of the order of nanometer. The operation of the LPG is on the basis of coupling the fundamental core mode to higher order co-propagating cladding modes. The coupling wavelength is obtained by the linear momentum conservation law or the phase matching equation $\lambda = (\beta_1 - \beta_2)\Lambda$, where β_1 and β_2 are the core and cladding mode propagation constants respectively and Λ is the period of the LPG (Kashyap, 1999).

FBG can be employed as a frequency selective reflector or a polarization selective rotator. In the reflector state, the forward modes are coupled to the backward modes. While in the polarization rotator, a mode with a definite polarization is coupled to another mode with different polarization. In the frequency selective reflector, coupling to the backward modes occurs in a narrow range of wavelengths around the wavelength for which Bragg condition is satisfied $\lambda = 2n_{eff}\Lambda$, where n_{eff} is the effective refractive index of the core. Bandwidth of FBG is typically below 1nm and depends on the amount of refractive index variation and the length of FBG. The governing equations of the FBG can be obtained from the conservation of energy and momentum (Kashyap, 1999; Chen, 2006).

Depending on the application of FBG, the period of the structure can vary in a definite way or randomly along the optical fiber core. This structure is named chirped FBG which has many applications in optical networks and sensors (Kashyap, 1999; Rao, 1997).

3. Basic optical fiber interferometer configurations

Interferometry is based on the superimposing of two or more light beams to measure the phase difference between them. Interferometer utilizes two light beams with the same frequency. Typically an incident light beam of interferometer is split into two or more parts and then recombine together to create an interference pattern. The integer number of wavelength for the optical path difference between the two paths corresponds to constructive points and odd number of half wavelengths corresponds to destructive points of the interference pattern. So in the output optical spectrum of the optical fiber

interferometer (OFI), the position of minimum can be shifted to maximum position if the optical path difference varies by odd number of half wavelengths. At least two optical paths are necessary for an interfererometery experiment. These optical paths can be in one optical fiber with two or more different optical fiber modes. Each of modes defines one optical path for the interferometer such as the Sagnac interferometer where the optical paths are defined by the clockwise and counter clockwise modes. The optical paths can be defined by separate optical fibers such as Mach-Zehnder OFI. There are many interferometer configurations that have been realized with the optical fiber. To see the principle of their operation, the detail of some interferometers such as Sagnac, birefringence OFI, Mach-Zehnder, Michelson, Moiré and Fabry-Perot interferometer are presented.

3.1 Sagnac optical fiber interferometer

The configuration of a Sagnac optical fiber is illustrated by Fig. 3. The optical source is a single mode stabilized coherent semi-conductor or Erbium doped optical fiber laser. The laser output beam is assumed to be well collimated with uniform phase. The laser beam enters the lossless 3dB optical fiber coupler (OFC). At the OFC the injected light splits into two parts with equal intensity that each of them travels around single mode optical fiber coil in opposite directions. The output of Sagnac coil is guided toward a single detector.

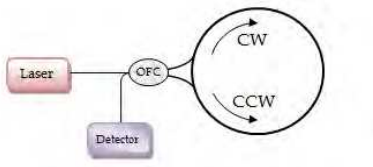

Fig. 3. A schematic diagram of Sagnac fiber interferometer.

Due to this specific configuration, fiber Sagnac interferometer has been used for rotation sensing primarily. In a non-rotating Sgnac interferometer, the clockwise (CW) and counter clockwise (CCW) modes are in phase while for a rotating Sagnac configuration due to the rotating velocity, the optical path of one of the modes is shorten and the other one is lengthen. The Sagnac effect causes the interference spectrum depends on the angular frequency of the setup (Sagnac, 1913). Analysis can be based on the Doppler frequency difference between the CW and CCW modes. The detector output frequency is the beating frequency of CW and CCW modes. When rotational axis is oriented along the optical fiber coil axis, the phase difference of CW and CCW modes is $\Delta\Phi = 8\pi NA\Omega/\lambda c$ (Burns, 1993; Vali & Shorthill, 1976), where λ is the free space optical wavelength, $'A'$ is the area of Sagnac coil, N is the number of the coil turn and Ω is the angular velocity. The sensitivity is the ratio of the phase difference to the angular velocity $S = 8\pi NA/\lambda c$, which is increased by increasing the coil radius, total fiber length and laser frequency. Optical fiber loss and packaging criteria limit the total fiber length and coil radius respectively.

Sagnac fiber interferometers can also be employed for sensing nonreciprocal and time-varying phenomena. So they become applicable tools for detection current, acoustic wave, strain and temperature. The optical gyroscope based on sagnac interferometer is commercially available (Bohnert et al., 2002; Lin et al., 2004; Starodumov et al., 1997; Dong & Tam, 2007; Fu et al., 2010)

3.2 Modal optical fiber interferometer

The modal interferometers are based on the difference between velocities of two different modes. Typically the first two modes of step index fiber like LP_{01} and LP_{11} or the HE_{11} and HE_{21} can be employed to design the modal interferometers. Also the two eigen polarizations of PMF are employed for modal interferometry (Bahrampour et al., 2012). The holy structure fibers have unique modal properties that are not possible with conventional optical fibers. Fig. 4 (a) and (b) show the cross section of high birefringence photonic crystal fiber (HiBi-PCF) and polarization maintaining photonic crystal fiber (PM-PCF) respectively (Villatoro, 2009).

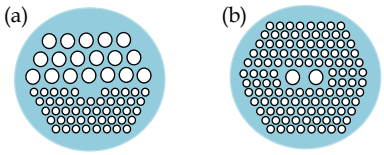

Fig. 4. Cross section of (a) HiBi-PCF (b) PM-PCF.

The PCFs have the possibility for the detection, sensing or spectroscopic analysis of gasses and liquids. In PCF a fraction of light penetrates into the voids for interaction and detection of gasses or liquids by spectroscopic methods (Villatoro et al., 2009). The holey and hollow fibers have their own advantages. Holey fiber which is filled with the desired gas or liquid, interacts with evanescent field which is only a few percent of total light power, while in hollow fiber, the fiber core is filled by gas or liquid and interacts with core light which is more than 90% of the total light power. The silica core single mode PCF bandwidth is more than one thousand nanometer which is much greater than those of an air core PCF fiber. A nano layer of rare metal coating on the surface of core and voids causes Plasmon-light interaction in PCF and extremely enhances the interferometer sensitivity (Hassani & Skorobogatiy, 2006). However the compact simple modal fiber interferometers depending on the fiber type such as Panda or birefringent PCF, can be employed in long lengths and short lengths applications (Villatoro et al., 2006).

3.3 Mach-Zehnder optical fiber interferometer

A schematic of conventional Mach-Zehnder OFI is sketched in Fig. 5.

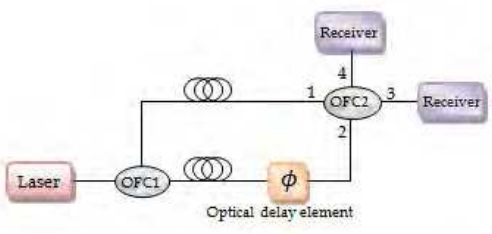

Fig. 5. A Schematic of optical fiber Mach-Zehnder interferometer.

By employing the commercial $(N \times N)$ coupler and single mode optical fibers, it is easy to construct the N-path interferometer. A schematic of N-path Mach-Zehnder interferometer is presented in Fig. 6. Each lossless linear multi port coupler is described by a $3N \times 3N$ unitary matrix. If N inputs and N outputs are linear polarized, linear coupler can be characterized by $N \times N$ matrix. As an example a symmetric 3×3 fiber coupler (tritters) which is commercially available, is described by 3×3 matrix (Weihs et al., 1996)

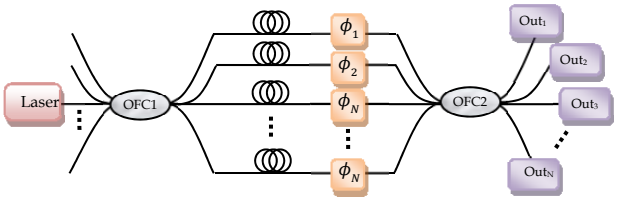

Fig. 6. A schematic configuration of N-path Mach-zehnder interferometer.

The 3-paths Mach-Zehnder interferometer is described by the product of two coupler matrices T and diagonal phase matrix $P = diag(e^{i\varphi_1}, e^{i\varphi_2}, e^{i\varphi_3})$ where φ_i(i=1,2,3) is the phase of the i-th path $(M = TPT)$. This analysis is restricted to beams with identical polarization thus a scalar analysis is sufficient. It is assumed that only one of the input fields is nonzero. So the input field vector is denoted by $E_{in} = (E_{1_{in}}, 0, 0)$. The output field $E_{out} = (E_{1_{out}}, E_{2_{out}}, E_{2_{out}})$ is determined by the Mach-Zehnder transformation matrix $E_{out} = ME_{in}$. The output intensities $I_n = |E_{n_{out}}|^2$(n=1,2,3) versus the input intensity $I_o = |E_{1_{in}}|^2$are given in the following:

$$I_n = \frac{I_0}{9}[3 + 2\cos(\varphi_{12} + \theta_n) + 2\cos(\varphi_{23} + \theta_n) + 2\cos(\varphi_{31} + \theta_n)];\ n = 1,2,3 \tag{1}$$

where $(\theta_1, \theta_2, \theta_3) = (0, -\frac{2\pi}{3}, \frac{2\pi}{3})$ and $\varphi_{ij} = \varphi_i - \varphi_j$ is the phase difference between the i-th and j-th branches. Above results are based on the loss-less fiber. For lossy fibers the phase matrix P is replaced by matrix $P' = diag(a_1, a_2 \exp(i\varphi_{12}), a_3 \exp(i\varphi_{13}))$ where a_n (n=1,2,3) is the transmission coefficient of the n-th optical fiber branch. The output intensities at the output of a 3×3 lossy Mach-Zehnder interferometer are:

$$\begin{aligned} I_n = \frac{I_0}{9}[&{a_1}^2 + {a_2}^2 + {a_3}^2 + 2a_1a_2\cos(\varphi_{12} + \theta_n) \\ &+2a_2a_3\cos(\varphi_{23} + \theta_n) + 2\,a_1a_3\cos(\varphi_{31} + \theta_n)];\quad n = 1,2,3 \end{aligned} \tag{2}$$

Similar to the interference pattern of the N-slit which is illuminated by a plane wave, there are $N - 2$ side lobes between the main peaks of interference pattern in the N-path fiber interferometer.

The sensitivity of an N-path interferometer is higher than the conventional Mach-Zehnder interferometer, because the slopes of main peaks are steeper. Mach-Zehnder interferometer can be used as a fiber sensor, because the phase difference can be changed by environmental effects such as strain. The light in the cladding is more sensitive to the surrounding changes than that in the core. The Long Period Grating (LPG) which can couple light from the core to the cladding or reverse is suitable to be employed in Mach-Zehnder fiber interferometer sensor. (Dianov et al., 1996)

3.4 Michelson optical fiber interferometer

A schematic of conventional Michelson OFI is depicted in Fig. 7. The high coherent light beam is split into two different optical paths in the upper and lower single mode optical fibers by the 2 × 2 optical fiber coupler (OFC). The light reflected back by mirrors M_1 and M_2 are recombined by the OFC to produce interference pattern at the receiver.

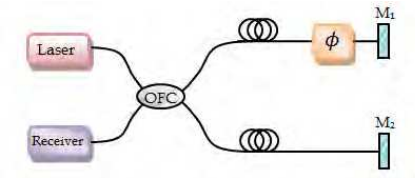

Fig. 7. A schematic configuration of Michelson OFI.

As shown in Fig. 8 by employing a $N \times N$ bidirectional coupler, the conventional Michelson OFI is generalized to the N-path Michelson OFI. Each ports of a $N \times N$ coupler can transmit incoming and outgoing waves simultaneously. Generally each linear bidirectional $N \times N$ OFC is characterized by a $6N \times 6N$ scattering matrix. In an analysis based on the identical polarization where a scalar analysis is sufficient, the scattering matrix becomes a $2N \times 2N$ matrix and denoted by Y. The incoming and outgoing electric field vectors are denoted by $E_{in} = (E_{in}^{(1)}, E_{in}^{(2)})$ and $E_{out} = (E_{out}^{(1)}, E_{out}^{(2)})$ respectively. $E_{in}^{(1)}$, $E_{out}^{(1)}$ and $E_{in}^{(2)}$, $E_{out}^{(2)}$ correspond to the $N \times 1$ vectors of the left and right ports of the $N \times N$ bidirectional coupler.

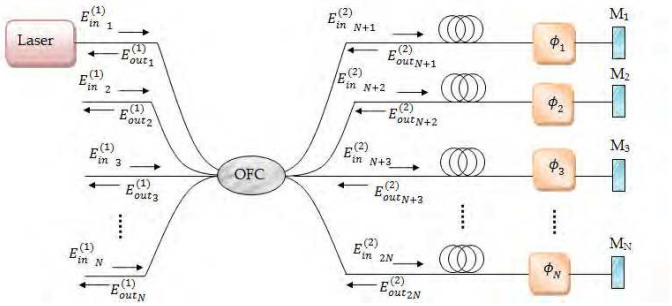

Fig. 8. A schematic configuration of N-path Michelson interferometer.

The incoming and outgoing vectors are related by $E_{out} = YE_{in}$ where Y can also be written in the block form:

$$\begin{pmatrix} E_{out}^{(1)} \\ E_{out}^{(2)} \end{pmatrix} = \begin{pmatrix} Y^{11} & Y^{12} \\ Y^{21} & Y^{22} \end{pmatrix} \begin{pmatrix} E_{in}^{(1)} \\ E_{in}^{(2)} \end{pmatrix} \tag{3}$$

where Y^{ij}(i,j=1,2) is a $N \times N$ matrix. For a lossless $N \times N$ OFC, Y is a unitary matrix. The diagonal matrix $P = diag\left(a_1^2, a_2^2 \exp(i\varphi_{12}), \ldots, a_N^2 \exp(i\varphi_{1N})\right)$ is the transfer matrix between the forward and backward waves in the optical fiber array. a_n is the transmission coefficient of the nth optical fiber and φ_{1n} is the phase difference between the phase accumulated by the field during the propagation in the nth and first optical fiber. The outgoing and

incoming fields of the right ports of the $N \times N$ OFC is related by the relation $E_{in}^{(2)} = PE_{out}^{(2)}$. By combining this relation and (3), the transfer matrix of the Nth path Michelson interferometer is obtained.

$$E_{out}^{(1)} = [Y^{11} + Y^{12}Y^{21}P(1 - Y^{22}P)^{-1}]E_{in}^{(1)} \tag{4}$$

It is assumed that only one of the input fields is nonzero. The input field vector is denoted by $E_{in} = (\varepsilon_{1_{in}}, 0,0, \dots, 0)$. The output intensities of the left ports are:

$$I_j = I_0\left|Y_{j1}^{11} + (Y^{12}Y^{21}P(1 - Y^{22}P)^{-1})_{j1}\right|^2, \qquad \mathrm{j} = 1, \cdots, \mathrm{N} \tag{5}$$

As mentioned in Mach-Zehnder OFI, it is easy to show that the sensitivity of multi-paths Michelson interferometer is greater than that of conventional two paths one.

3.5 Optical fiber Moiré interferometery

Moiré interferometry is based on the fringe pattern formed by overlaying two or more gratings at different angle θ. The desired fringe pattern can also be designed by a suitable arrangement of optical fibers. The optical fiber based generator of interference grid pattern, is configured by N polarization maintained fibers. The coordinates of the center of the jth fiber in the plane $z = 0$ is denoted by $(a_j, b_j), (j = 1, \dots, N)$. The polarization angle of the jth fiber relative to the x axis is denoted by θ_j $(j = 1, \dots, N)$. The field at the point (x, y) in the $z = D$ plane is given by:

$$E = \sum \overrightarrow{E_j} e^{-i[\frac{k}{D}(xa_j + yb_j) + \varphi_j]} \quad + c.c. \tag{6}$$

where φ_j is the phase of the jth fiber at the $z = 0$ plane. The field intensity at the point (x, y) in the observation plane is as follows:

$$I = \sum_{i=1}^{N} I_i + \sum_{i \neq j} \sqrt{I_i I_j}\, cos(\theta_i - \theta_j)\, cos\left\{\frac{k}{D}\left[(a_i - a_j)x + (b_i - b_j)y\right] - \varphi_{ij}\right\}, \tag{7}$$

where $I_i (i = 1, \dots, N)$ is the light intensity corresponding to the ith fiber at point (x, y), φ_{ij} is the phase difference between the ith and jth optical fibers and k is the light wave number. (Yuan et al., 2005). By suitable choosing of the parameters $a_i, b_i \; and \; \theta_i \; (i = 1, \dots, N)$, the desired fringe configuration can be obtained. As an example consider a system of three fiber centered at $P(0,0), P(2a, 0)$ and $P(0,2a)$, where $'a'$ is the radius of the polarization maintained fiber. Fig. 9 shows the arrangement of the interference pattern generator. The interference pattern of three fibers with the same polarization direction is shown in Fig. 9 (a). The vertical and horizontal patterns correspond to the interferences of fibers 1 and 2 and fibers 1 and 3 respectively. The oblique lines families in Fig. 9 (a) are due to the interference of the fibers 2 and 3. As shown in Fig. 9 (b), by employing the vertical and horizontal polarization for the fibers 2 and 3 respectively and setting the angle 45° between the polarization of fiber 1 and x-axis, the oblique lines are eliminated. The inverse problem is to design a suitable configuration of PMF optical fibers to obtain a desired intensity distribution $I(x, y)$ or fringe pattern. By defining a suitable meter on the intensity distribution space and employing the optimization techniques such as variational method and genetic algorithm, it is possible to minimize the distance between the generated distribution and the desired distribution.

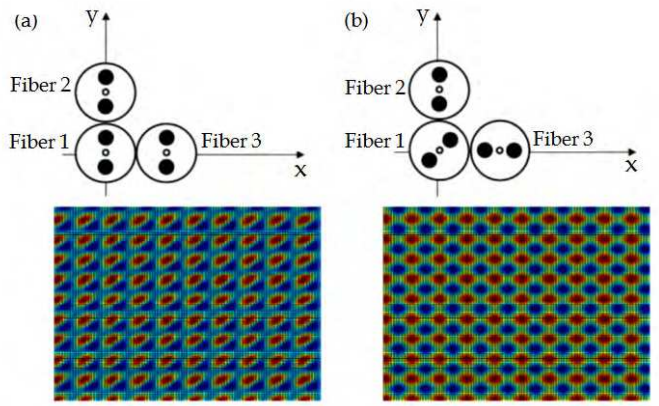

Fig. 9. Two arrangements of optical fiber Moiré interferometer and their interference patterns. a) The polarizations of the three fibers are in the same direction b) fibers 2 and 3 with vertical and horizontal polarization and fiber 3 with angle 45°.

3.6 Optical fiber Fabry-Perot interferometer

A Fabry-Perot (FP) consists of two optically parallel reflectors with reflectance $R_1(\omega)$ and $R_2(\omega)$ separated by a cavity of length L. Reflectors can be mirrors, interface of two dielectrics or fiber Bragg gratings. The cavity may be an optical fiber or any other optical medium.

Two different optical fiber Fabry-Perot interferometers are shown in Fig. 10.

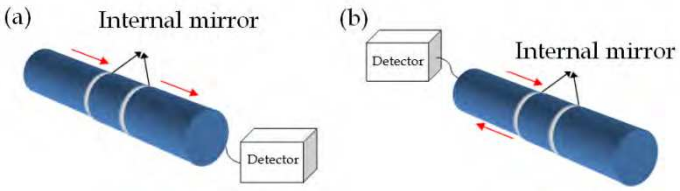

Fig. 10. (a) Fabry-perot based on the light transmission (b) Fabry-perot based on the light reflection.

One is based on the light transmission through a Fabry-Perot, while the other is based on the reflection. Due to multiple reflections, the reflected and transmitted spectrums are functions of cavity length, medium index of refraction and mirrors reflectivity. Because of energy conservation law, the transmitted spectrum is opposite to the reflected spectrum.

Optical fiber Fabry-Perots are classified as intrinsic and extrinsic types. In the intrinsic fiber FP interferometer (IFFPI), the two mirrors are separated by a single mode fiber, while in the extrinsic fiber FP interferometer (EFFPI), the two mirrors are separated by an air gap or by some solid material other than fiber. In both IFFPI and EFFPI, light from emitter to the FP and from FP to the detector are transmitted by a single mode fiber. Fig. 11 shows schematic configurations of three IFFPI. One end of the fiber shown in Fig. 11 (a) is polished as a mirror. For higher reflection the polished end is coated with switchable dielectric layers. The

second mirror of IFFPI shown in Fig. 11 (a) is an internal mirror which can be produced by splicing of polished fibers or by polished coated fibers. Both mirrors of the IFFPI shown in Fig. 11 (b) are internal fiber mirrors while those are used in the IFFPI presented in Fig. 11 (c) are FBG reflectors. Depending on the application of IFFPI, one of the configurations presented in Fig. 11 can be used.

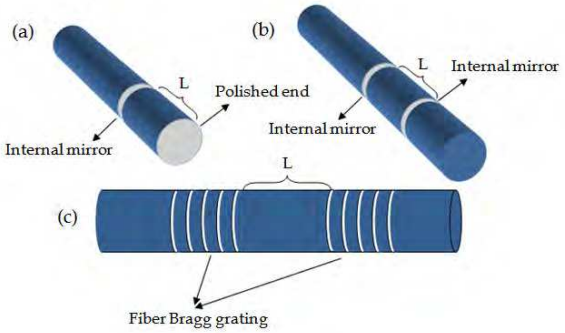

Fig. 11. Schematic configurations of three IFFPI.

Four different EFFPI configurations are shown in Fig. 12.

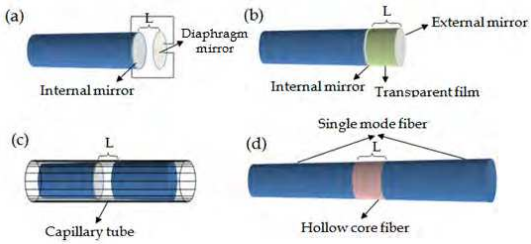

Fig. 12. Schematic configurations of four EFFPI.

In Fig. 12 (a) the air-gap cavity is bounded by the end of a polished fiber and a diaphragm mirror. The cavity length is of the order of several microns and can be increased by convex mirror diaphragm. In another configuration presented in Fig. 12 (b) a thin film of transparent solid material is coated on the end of the fiber. The air-gap cavity between two polished fiber surfaces, where the fibers are aligned in a hollow tube is another configuration of EFFPI (Fig. 12 (c)). The structure shown in Fig. 12 (d) is called the in-line fiber etalon (ILFE). The ILFE is constructed of a hollow-core fiber spliced between two single mode fibers. The diffraction loss causes to limit the practical length of EFFPI to a few hundred of microns (Shizhuo, 2008).

3.7 White light fiber interferometry

The interferometric techniques are known as the precise method for measuring physical quantities that can induce the optical path difference (OPD) in the interferometers. The

coherent length of the narrow band sources such as Lasers are greater than the optical path length difference in the interferometers. Due to the periodic nature of the interferogram fringes, the interferometric measurement suffers from an integer multiple of 2π phase ambiguity. Hence interferometers driven by narrow line-width Lasers do not produce absolute data unless extra complexity is added to the interferometer. By employing the short coherent light that is illuminated from wide-band light sources, the phase ambiguity is eliminated. In wide bandwidth interferometer the fringes of the interferogram are narrowly located in the zero path length difference region (Flourney et al., 1972). So the phase difference can be determined without the phase ambiguity by measuring the fringe peak or the envelop peak of the interferogram. This type of interferometry is named as white light or low coherence interferometry. In white light interferometry (WLI) corresponding to each wavelength a separate fringe system is produced. The electric field at any point of observation is the sum of electric fields of these individual patterns. In a WLI which is adjusted such that the optical path difference is zero at the center of the field of view, the electric field of different wavelengths exhibits the maximum at the center point. The fringes of different wavelengths will no longer coincide as moving away from the center of the pattern. The fringe pattern is a sequence of colors whose saturation decreases rapidly. The central bright white light fringe can be used to adjust the WLI.

The light sources such as fluorescent lamp, SLDs, LEDs, Laser diodes near threshold, optically pumped Erbium-doped fibers and tungsten lamps, can be used in the WLI. The spectral width of SLD and LED is between 20 and 100 nm. It is expected that at the operating wavelength (1.3 μm) of these types of light sources, the coherent length is between 17 and 85 μm. Because of the wave-train damping, the Doppler effect, disturbances by neighbor atoms, noises and mode mixing effects, the practical coherent length is less than those are predicted previously.

In the WLI, one of the two arms is used as the measurement arm and the other one as the reference arm. The length of the reference arm can be controlled by different methods such as moving mirrors or Piezoelectric (PZT) devices. Generally the operation of WLI is based on the balancing the two arms of the interferometer and compensating the OPD in the measurement arm. Therefore the desired measurement can be achieved.

As the OPD between the two paths of a WLI is varied, the intensity of interference fringe drops from a maximum to a minimum value. The maximum intensity corresponds to the central white bright fringe. Measurement of the position of the central fringe in the WLI is of prime importance. Because the distance between the central fringe and its adjacent side fringes is too small and the presence of noise, the determination of the central fringe position is inaccurate, so there are some ambiguities in the central fringe identification. This problem can be solved by employing a combinational source of two or three multimode Laser diodes with different wavelengths.

White light fiber interferometers (WLFI) can be designed on different topologies of single or multi-mode fiber interferometers. Each of the single mode and multi-mode fibers has their own advantages and disadvantages. For example usually white light single mode fiber interferometer provides stable and large signal to noise ratio while in the interferometers based on multi-mode fiber, cheaper optical components are employed (Song et al., 2001; Manojlovi et al., 2010). Generally there are several WLI topologies corresponding to the

standard optical fiber interferometer and their combinations (Yuan, 2002; Mercado et al., 2001;). As an example Fig. 13 shows a white light fiber optic Michelson interferometer working in the spatial domain. The LED light is coupled to the two path of Michelson interferometer through a 2 × 2 OFC without insertion loss. The reflected beams recombine on the PIN detector of the WLI. The scanning mirror is adjusted for maximum output corresponding to the position of central fringe.

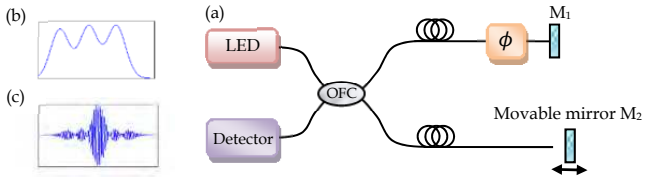

Fig. 13. (a) A schematic configuration of WLI Michelson interferometer (b) Input LED spectrum (c) Interference fringe pattern.

As shown in Fig. 13(c) for OPD less than the source coherence length, the white-light fringe pattern is produced. The position of the highest amplitude corresponds to the exactly zero optical path difference between two beams. After some mathematical manipulations for LED parameters presented in (Yuan, 1997), the normalized interference fringe pattern is calculated and result is presented in Fig. 14. The results of three peaks LED are compared with those of a normal LED to see how the multi wavelength white light source increases the precision of the central fringe position measurement relative to the single white light source.

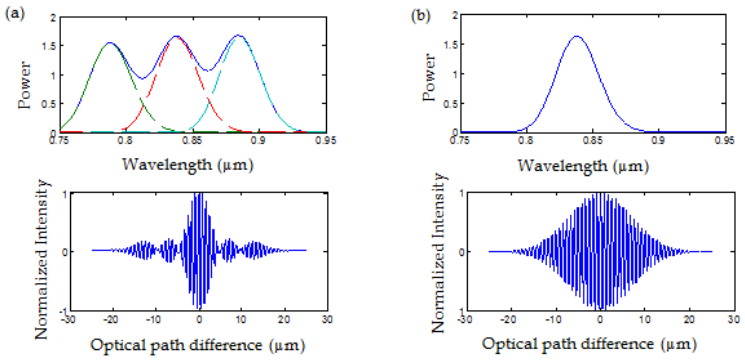

Fig. 14. The spectrum distribution of the light source (up) and their normalized interference fringe pattern (down) (a) Three peaks LED (b) Normal LED.

4. Signal recovering methods

The phase difference between two coherent light beams is detected by interferometric methods, which are most sensitive techniques for optical path difference measurement. The OPD variations have sufficiently low frequency components. So when they are converted to

the light intensity on the observation plan, they can easily be detected by photo diodes, photo diode matrix or charge coupled devices (CCD). The detector output is proportional to $cos(\phi)$, where ϕ is the phase difference. In the presence of cosine and the absence of sinusoidal signal an ambiguity exists in the phase recovering. If the phase amplitude falls outside the (0 to 2π) range, in addition to sine and cosine values we must track the history of phase angle variation to know in which quadrant it precisely lie. Numerous methods have been devised for recovering the path length difference from the output signals of OFI. The methods based on the production of new frequencies are called heterodyne detection otherwise are named homodyne methods. The main three methods are briefly described in following.

4.1 Phase generated carrier (PGC) homodyne detection

In this method the interferometer Laser source is driven by combination of direct and sinusoidal current. The Laser output power and wavelength are modulated by the Laser current variation. In the presence of path length difference, the change of the wavelengths indicates itself as a change in the output phase. The current frequency can be observed in the received phase in the output. Each of the current frequency and its harmonics carries in their sidebands a copy of the created phase modulated signal. Two of these copies are chosen by band pass filters. Proper control of the amplitude of the sinusoidal current and filters configuration guaranty that the chosen copies have the same amplitude. The filters outputs are used as the inputs of an electronic mixer. One of the outputs of the mixer is proportional to sine, while the other one is proportional to the cosine of the interesting signal. Sometimes the method is also called Pseudo-Heterodyne Detection (PHD) (Jackson et al., 1982).To produce the phase shift instead of Laser frequency modulation it is possible to create phase shift with a cylindrical Piezoelectric, which is wrapped around one arm of the interferometer and is derived with a sinusoidal voltage (Hoeling et al., 2001). This case is called synthetic heterodyne method (Strauss, 1994).

4.2 Fringe-rate methods

When large phase shift is produced in an interferometer, two new methods which are called fringe-counting and fringe-rate demodulation become feasible (Barone et al., 1994; Crooker & Garrett, 1987). These methods are based on the transitions of interferometric outputs across some central value. In the fringe counting method, on a suitable period of time the transitions are counted digitally. The instantaneous frequency is determined by the ratio of the counting number to the counting time. Because in practice one must wait a short time to obtain at least one count, it is impossible to obtain an instantaneous count. However the phase can be obtained by integrating the instantaneous frequency. In the fringe-rate method, the transitions are used as inputs of a frequency to voltage converter circuit (FVC). To obtain the phase difference, the output of FVC circuit is integrated. There is no transition for weak signal. The minimum detectable signal is of the order of π radian.

4.3 Homodyne method

The operation range of the synthetic heterodyne method is limited above to π radian, while the fringe-counting and fringe-rate techniques are limited from below to π radian (Dorrer et al., 2001). A number of homodyne techniques are employed to bridge this region. All these

methods are based on the use of orthogonal components without using heterodyne methods. OFIs usually have two outputs. A 2×2 OFC is employed to combine the two path beams of the interferometer and form the interference pattern. By energy conservation law it is easy to show that the two outputs are 180° out of phase from one another. When one output is dark, all energy must be presented in the other output and vice versa. So no orthogonal components can be found in the outputs. The orthogonal components are produced by the heterodyne methods. The output coupler can be modified such that the orthogonal components directly exist in the outputs. As an example a 3×3 coupler can be employed as the output coupler of the interferometer to create output with orthogonal components without employing the heterodyne detection method (Choma et al., 2003).

5. Noise sources in optical fiber interferometers

Calculation of signal to noise ratio strongly depends on the OFI topology. In principle the noise sources belong to the light source, optical fibers, detector, electronic circuits and environment (Bottacchi, 2008; Tucker & Baney, 2001). Moreover any random process in each stage of interferometry: signal generation, transmission and detection can be considered as a noise source.

The laser generation is the result of the quantum interaction of electromagnetic wave and matter. The spontaneous and stimulated emissions are quantum effects and are the noise sources in the phase and amplitude of laser output (Linde, 1986; Clark, 1999; Tsuchida, 1998). On the other hand the interaction of light with universal modes of surrounding reservoir through the mirror coupling and stimulated emission in active medium bath are also noise sources for the laser output (Scully & Zubairy, 2001). The cavity filtering and feedback can reduce the laser noise significantly (Sanders et al., 1992; Cliché et al., 2007). The phase and amplitude of laser noise cause to increase the bandwidth of the laser light. In single mode lasers by proper design of optical cavities, the bandwidth can be reduced to several kilohertz, which gives several tens of kilometers for coherent length. The mode competition and cross saturation effects are new noise sources in multimode lasers that can be employed in wide band fiber interferometry.

Rayleigh scattering, Mie scattering, core cladding interface scattering, Brillouin scattering, absorption and amplification parts in the optical fiber, are the main noise sources in OFI arms and transmission parts. Some parts of the scattered light are trapped in the guided region and travel in both direction of the fiber, contribute to the phase and amplitude noises. Other parts are scattered out of the optical fiber and affect the amplitude noise only. Except the Brillouin and Raman scatterings, all other effects are linear and do not change the light frequency. Both the Brillouin and Raman scattering have two different components Stokes and anti-Stokes frequencies. The Stokes and anti-Stokes Brillouin shifts are due to the light-acoustic phonon interaction and are about ± 25 GHz, while the Stokes and anti-Stokes Raman shift correspond to the optical phonon-photon interaction and are of the order of 13 THz (Agrawal, 2007). Beating between Stokes, anti-Stokes and direct beam can occur, but such a high beating frequencies cannot be observed at the output response of any realistic detector and are eliminated intrinsically by the low pass filter detector. The Brillouin and Raman scattering loss can be considered as a source of amplitude noise. The Rayleigh, Brillouin and Raman scattering are symmetrically distributed with respect to the forward

and backward direction while those of Mie and core-cladding interference scattering are mainly in the forward direction.

Mode coupling is another source of noise in multimode fiber interferometer. In such an interferometer the mode coupling noise must be taken into account. Absorption and amplification correspond to the interaction of light with reservoirs so according to quantum Langevin equation there are some noises in the output (Scully & Zubairy, 2001). Generally Avalanch photo diode (APD), PIN diode, charge coupled device (CCD) and photo multiplier (PM) are used as the electronic detector of the OFIs. Dark current noise, shot noise, background noise, thermal noise and flicker noise are common in all of the optical detectors. The generation and recombination of electron hole are a stochastic process in semiconductor detectors and are the noise sources of such detectors. The avalanche effect, the basis of operation of APDs is a random process and causes noise generation in avalanche photo diode. The same effect on the anodes of PM can be a noise source in PM detectors. The amplifier noise which is consistent of the shot noise, Johnson noise, burst noise and flicker noise of different solid state electronic elements of the amplifier is the final intrinsic noise of OFI.

The fiber parameters can be affected by the environmental physical variations such as mechanical vibration, acoustic agitation, pressure, tension and thermal variations. In a controlled way this effects can be used to make the optical fibers as a sensor for these physical quantities, while in OFIs are noise sources. As an example the population of Stokes and anti-Stokes photons are functions of the fiber temperature and can be used to design a high precision temperature sensor for water, oil and gas leak detection systems (Harris et al., 2010; Chelliah et al., 2010). The Stokes and anti-Stokes parameters of Brillouin scattering are functions of fiber strain and fiber temperature. This effect is used to measure the strain and temperature simultaneously for structural health monitoring systems (Güemes, 2006; Bahrampour & Maasoumi, 2010). The optical fiber sensitivity to mechanical variation and acoustic waves are employed for various applications such as acoustic, vibration and ultrasonic detectors for under water sensor systems. However the output signal is affected by all the noise sources and the aim is to denoise signal by the signal processing methods. Depending on the signal, one of the denoising methods such as Fourier regularized deconvolution (ForD) and Fourier wavelet regularized deconvolution (ForWaRD) method can be employed (Bahrampour & Askari, 2006; Bahrampour et al., 2012). The wavelet deconvolution method generally use to denoise transient signals. The short time Fourier method is employed to denoise the music-like signals of a fiber intruder detector based on the birefrigent fiber interferometer (Bahrampour et al., 2012).

6. Applications of optical fiber interferometers

Optical fiber interferometers as a precise measuring interferometer or sensitive tools have many applications in all branches of science and technology (Shizhuo et al., 2008). The OFIs can be employed to design the optical components for the inline signal processing, such as band pass filters in optical communication networks. The same topologies can be easily fabricated by the light waveguides in the integrated circuits by means of photolithographic process for application in optical transmitters and receivers. Because of high sensitivity of the interferometer, the linear and nonlinear properties of optical fiber can be detected. These

properties make long length and short length waveguide and fiber interferometer sensors, suitable in novel applications such as oil and gas pipeline monitoring, temperature distribution measurement in the depth of ocean and intruder sensors. Among the wide range of applications of waveguides and fiber interferometers, only a few applications in the optical communication networks and special types of fiber and waveguide interferometric sensors are mentioned in this section.

6.1 Applications in optical fiber networks

The key devices in optical DWDM communication networks are re-amplifying, re-shaping and re-timing (3R-regenerator) systems. In re-shaping and re-timing circuits the nonlinear networks such as clipper, clampers, switching and flip-flops are of prime importance. While in add-drop filters, the linear filters such as tune and notch filters have an important role. On the basis of a nonlinear Mach-Zehnder interferometer, the structure of an all optical inverter is shown in Fig. 15.

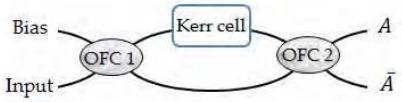

Fig. 15. A schematic of an all optical inverter. OFC is an optical 2 × 2 coupler.

An optical fiber with high nonlinear Kerr effect such as Chalcogenide glasses is employed in one of the Mach-Zehnder interferometer arms. So in the presence of a suitable light intensity at the input of optical fiber coupler 1 (OFC 1), the change of refractive index ($n = n_0 + nI$) causes a π-phase shift in the upper arm of the interferometer relative to the lower arm. It is assumed that in the absence of the input, the interferometer arms are balanced and the outputs A and $\bar{A}$ are in the constructive and destructive conditions respectively. The 0 and 1 digital states are represented by destructive and constructive output ports. In the presence of the OFC 1 input, the output A changes to 0 and the $\bar{A}$ switches to 1. This interferometer is an optical logic inverter. The structure shown in Fig. 15 is also used in quantum non-demolition experiments (Gerry & Knight, 2005). For small input intensities Fig. 15 acts as an intensity modulator circuit and $\bar{A}$ output is approximately proportional to the input intensity. By varying input intensity, the output varies from its maximum value to zero, i.e. this circuit operates as a light controlled variable attenuator.

The inverter of Fig. 16 is designed on the basis of optical waveguides to avoid the high length nonlinear optical fibers in the inverter design.

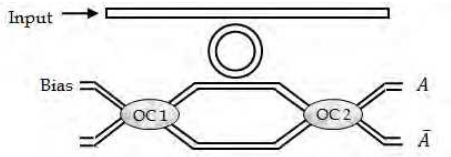

Fig. 16. A schematic of an inverter based on an optical waveguide and micro-ring resonator. OC is 2×2 optical coupler.

As shown in Fig. 16, the Kerr cell that is shown in Fig. 15 is replaced by a high dispersive nonlinear element such as micro-ring or microsphere. The phase difference between the input and output of micro-ring can be changed by the resonance frequency of the micro-ring which is controllable due to the cross-Kerr effect. The upper input to the micro-ring causes to change the micro-ring refractive index and therefore the resonance frequency is changed. So the phase difference between the input and output of the upper arm of the interferometer is changed. On the basis of optical fiber and optical waveguide interferometers in combination with ultrahigh nonlinear optical elements (UHNO), such as semiconductor optical amplifiers (SOA), different high frequency optical classical logic gates are designed and demonstrated. Also quantum interferometers such as Hong-Ou-Mandel interferometer are employed to design quantum gates (Hong et al., 1987; Olindo et al., 2006).

The bi-stability effect is the basis of the clipper and flip-flop circuits. Most bi-stability designs include both a cavity with nonlinear medium and a feedback (Bahrampour et al., 2008a, 2008b, 2008c). A novel OFI with common mode compensation is proposed by Backman (Backman, 1989). The Backman interferometer consists of a Mach-Zehnder interferometer with one nonlinear path and re-circulating delay line as shown in Fig. 17. The output intensity $|E_{out}|^2$ versus the input intensity $|E_{in}|^2$ in the steady state has the bi-stability behavior.

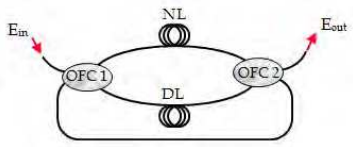

Fig. 17. A schematic of Backman interferometer. NL is nonlinear line and DL is delay line.

Flip-flops are building blocks of the sequential logic circuits such as time recovering circuits. As usual a reset-set (RS) flip-flop can be designed on the basis of regenerative feedback in the two inverter circuit. Fig.18 shows a RS flip-flop based on the two Mach-Zehnder interferometer inverters. The optical fiber couplers OFC 1 and OFC 2 are 3 × 3 couplers and OFC 3 and OFC 4 are 2 × 2 couplers. The bias light inserts to the upper and lower Mach-Zehnder interferometers (MZI 1, MZI 2) by a 2 × 2 coupler. R and S are the reset and set trigger inputs. A , $\bar{A}$ and B , $\bar{B}$ are the outputs of MZI 1 and MZI 2 respectively. Due to the energy conservation law, $\bar{A}$ and $\bar{B}$ are the logic complement of A and B outputs. In the absence of set and reset $A = B = 1$. The output complement of each inverter is connected to the control input of the other inverter. This network of Fig.18 has two stable ($A = 0, \bar{B} = 1$) and ($A = 1, \bar{B} = 0$) states. In the presence of trigger signal at S or R inputs, this system can switch between these two stable states.

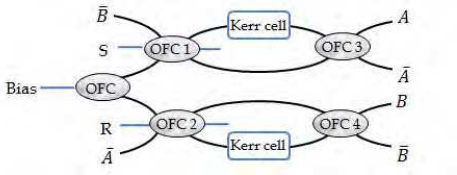

Fig. 18. A schematic of an optical Flip-Flop by combination of two Mach-Zehnder Interferometers.

In addition to the logic gates and nonlinear circuits, the fiber interferometers can be used to design linear circuits such as different types of optical filters. In many applications such as selection of a narrow spectrum from a broad band spectrum, band pass filter is of prime importance. Due to the Bragg diffraction effect, each FBG fiber can be used as a notch or band stop filter. As shown in Fig. 19, an optical coupler is employed to detect the reflected spectrum of FBG. In this filter, the input power splits into two parts by the OFC. The light reflected by a FBG is again equally split between the ports 1 and 2. Hence only 25% of the light is in the output port 2 of the band pass filter (Kashyap, 1999).

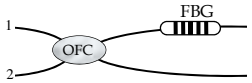

Fig. 19. A schematic of band pass filter.

To eliminate the insertion-loss of the band pass filter several interferometric methods was proposed (Kashyap, 1999). On the basis of Michelson, Mach-Zehnder and Fabry-Perot interferometers three different design of band pass filters are presented in Fig. 20(a-c) respectively(Kashyap, 1999).

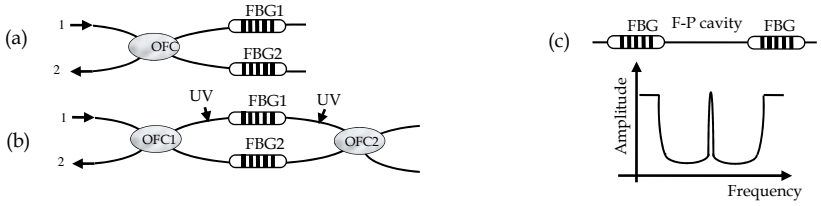

Fig. 20. Interferometric design of band pass filter (a) Michelson (b) Mach-Zehnder (c) Fabry-Perot.

In both arms of Michelson interferometer as shown in Fig. 20(a) a FBG is employed. The arms of Michelson interferometer are designed in such a way that the reflected light from FBG 2 arrives at the input port of OFC, has π out of phase with respect to the light reflected from FBG 1. In such a condition light from FBG 1 and FBG 2 interfere constructively at the output port 2, so that 100% of the light at the Bragg wavelength appears at the output port of band pass filter (Kashyap, 1999). The band pass spectrum can be designed by the profile of chirped spectrum. The dual grating Mach-Zehnder interferometer band pass filter as shown in Fig. 20 (b) is designed for the application in add-drop filters. The principle of operation is the same as that is demonstrated in Michelson band pass filter. Here "UV trimming" is used to balance the interferometer after the gratings are written. "UV trimming" relies on photo induced change in the refractive index to adjust the optical path difference. The simplest band pass filter is an inline Fabry-Perot interferometer. In distributed feedback (DFB) lasers, two FBG can be employed instead of mirrors. As shown in Fig. 20(c) a single $\lambda/4$ phase-shifted FBG has a sharp Lorentzian line shape band pass in the middle of band stop. The broader transmission band width is obtained by cascading several structure (Haus & Lai, 1992). Number of band pass peaks that they appear within the band stop increases by increasing the gap between the two grating sections.

6.2 Some applications in optical fiber sensors

The traveling wave in the dielectric medium of optical fibers and waveguides can be perturbed by their environment. This is the basic idea of the optical fiber sensors (OFS). The interaction of quantity of interest (which is called the measurand), with the optical fiber produces a modulation in the parameters of propagating light beam within the fiber. Generally there are four beam parameters for measurand modulation:

I) Intensity modulation: the intensity modulated fiber sensors are simplest and low cost fiber sensors for measuring the position, pressure and vibration in medical and industrial applications (Polygerinos et al., 2011, Jayanthkumar et al., 2006). Fig. 21 shows a distributed oil leak detection system based on intensity modulated sensor (Carrillo, 2002). The leaked oil causes to expand the polymer around the optical fiber. Due to the wrapped strain-less steel wire, the fiber bending loss increases and the oil leakage position can be measured by a commercial optical time domain reflectometer (OTDR) (Righini et al., 2009).

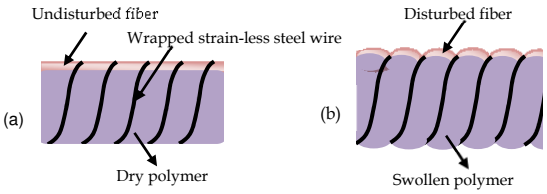

Fig. 21. Distributed Oil leak detection system.

II) Wavelength modulation: The measurands such as temperature and strain can be modulated on the resonance frequency of an inline Fabry-Perot or Bragg wavelength of an inline LPG. An optical or chemical transducers joint at the end of a fiber can be used as the wavelength modulator. Interaction of the measurand with transducer causes to change the spectral properties of transducer. The measurement of the optical spectrum of the transducer through the optical fiber makes possibility to monitor measurand status (Righini et al., 2009).

III) Polarization modulation: In birefringent optical fibers the two fundamental modes propagate with slightly different phase velocities. On the basis of high birefringent fibers several methods for current and magnetic field measurement are designed and manufactured. Fig. 22 shows the principle of operation of an intrusion sensor based on the birefringent optical fiber (Bahrampour et al., 2012).

An x-polarized ramped frequency modulated laser is injected to the birefringent fiber sensor. At the cross point of the intrusion and the fiber sensor, energy from the x-polarized mode is converted to the y-polarized mode. Due to different velocities of the x- and y-polarized modes a beating frequency is observed at the output of the detector. The intrusion position can be obtained from the output beating frequency.

The optical fiber and waveguide sensors that have been investigated and proposed for science, industrial, military, biochemical, biomedical, environment, automotive, avionic and geophysical applications are countless. One of the basic characteristics of the optical fiber sensors is their ability for long length distributed sensing. One of the most popular

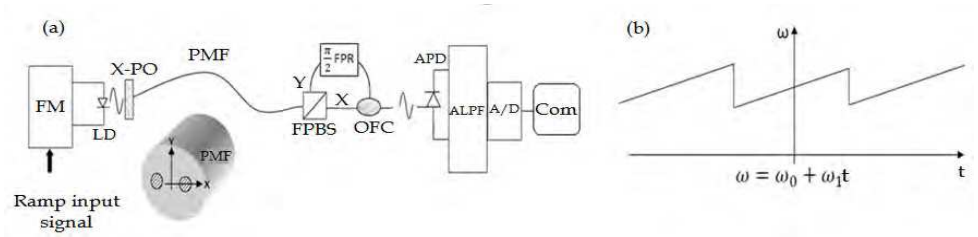

Fig. 22. A schematic of a birefringent fiber intruder detection system. FM is the frequency modulator, LD is laser diod, x-po is a x-polarizer, FPBS is a fiber polarization beam splitter, FPR is a fiber polarization rotator, APD is an avalanche photo-diode detector, ALPF is an active electronic low pass filter, A/D is an analog to digital convertor, Com. a computer system for signal processing and denoising. (b) Ramp input to the FM system (Bahrampour et al, 2012).

distributed fiber sensors is optical time domain reflectometer (OTDR) which is based on the monitoring the Rayleigh back scattering along the fiber. On the basis of Raman and Brilliouin scattering the OTDR is developed to the Raman time optical domain reflectometer (ROTDR) and Brillouin optical time domain reflectometer (BOTDR) respectively. The OTDR, ROTDR and BOTDR optical fiber sensors have applications in structural health monitoring (Glisic & Inaudi, 2008). In the absence of any intrusion, the ΦOTDR signal is saved in an electronic memory and it is compared with the ΦOTDR output continuously (Juarez et al., 2005). Due to the elasto-optic effect, in the presence of an intrusion, the fiber refractive index and hence the phase of the back scattered signal changes. This phase changes can be measured at the sensor output (Righini et al., 2009).

IV) Phase modulated sensors: Variation of the optical length of optical fiber causes a phase shift of the light beam $\Delta\phi = 2\pi(n\Delta L + L\Delta n)/\lambda_0$, where λ_0 is the free space light wavelength and n is the fiber refractive index. Phase shifts usually are measured by interferometric methods. Refractive index and fiber length can vary due to the characteristic of various measurands and therefore the cross sensitivity occurs. To avoid the cross sensitivity, special design of jacketing is necessary. The material of the jacketing is chosen such that to improve the effect of desired measurand and attenuates the others. A schematic of an optical fiber intrusion detector system is presented in Fig. 23. The light laser source through an optical circulator and a 50:50 coupler is connected to a Faraday rotating mirror (FRM). The intrusion distance (L_x) is the length between the intrusion point and FRM. The parts 3 and 4 of the coupler are connected with a fiber of length L_d to form a delay loop. The returned light through the port 1 of 50:50 coupler and circulator is transported to the detector . The intrusion point is determined after signal processing. There are four different paths in the system for transmission of light from source to detector:

Path I: $1 \rightarrow 2 - FRM - 2 \rightarrow 3 \rightarrow L_d \rightarrow 4 \rightarrow 1$

Path II: $1 \rightarrow 4 \rightarrow L_d \rightarrow 3 \rightarrow 2 \rightarrow FRM \rightarrow 2 \rightarrow 1$

Path III: $1 \rightarrow 2 \rightarrow FRM \rightarrow 2 \rightarrow 1$

Path IV: $1 \rightarrow 4 \rightarrow L_d \rightarrow 3 \rightarrow 2 \rightarrow FRM \rightarrow 2 \rightarrow 3 \rightarrow L_d \rightarrow 4 \rightarrow 1$

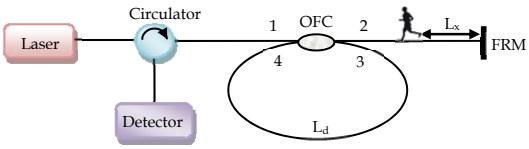

Fig. 23. A schematic of an optical fiber intrusion detector system.

All path differences except the optical path difference of the path I and II are so large, so they have no effect on the interference signal. The electric field at the photo detector is the superposition of the electric field corresponding to the four different paths. The time dependence of the strength of an intrusion at the detector and the instant t is $\Delta q = \Delta\varphi_0 sin\omega_s t$, where $\Delta\varphi_0$ and ω_s are the induced amplitude and frequency by intruder respectively. The light intensity of interference of electric field of path I and path II on the photo detector is easily obtained.

$$I_{in} = 2E_0^2 cos\left\{4\Delta\varphi_0 sin\frac{\tau_2\omega_s}{2} cos\frac{\tau_1\omega_s}{2} cos\omega_s(t-t_0)\right\}, \tag{8}$$

where $\tau_1 = 2nL_x/c$, $\tau_2 = 2nL_d/c$ and $t_0 = (\tau_1 + \tau_2)/2$. The relative amplitude of the frequency components of the detector outputs are functions of the intrusion distances and can be obtained by the Fourier transform method (Jia et al., 2008).

According to the general relativity, gravitational waves (GW) are produced when the curvature of spacetime disturbed by accelerating mass. The ripples in the curvature of spacetime propagate at the speed of light. A GW causes a tiny time dependent quadruple change of strain in the plane transverse to the wave's propagation direction. The space is stretched in one direction while is shrunk along its perpendicular direction. The strength of GW 'h' is expressed by the dimensionless strain $\delta L/L$. Due to the quadruple nature of Michelson interferometer, it is suitable device for gravitational wave detection. The interference pattern is linear measure of the strain. The amplitudes of GWs radiated from astrophysical sources at Earth are typically of the order of 10^{-21} or smaller. Detection of such weak strains needs high sensitive devices. For increasing the sensitivity of the interferometer, the lengths of the interferometer arms were increased to the order of kilometers and multi-path cell or Fabry-Perot optical cavity was used in each arm. So the light can be stored for a time comparable to the time scale of GW signal. Long base line gravitational wave detectors such as LIGO, VIRGO, GEO and TAMA are now operational. In the presence of GW, the change in the length of arms is very small. Hence many noises such as seismic noise, thermal noise and quantum noise limit the sensitivity of interferometer. Quantum noise is the fundamental and unavoidable noise in new generation of these interferometers and is due to the light-interferometer interaction. So the sensitivity of laser GW detector depends on the quantum state of light. It was shown that depending on the parameters of interferometer such as arm's lengths, frequency of laser and mass of mirrors, the optimum quantum state for the dark port is vacuum squeezed state with specific squeezing factor. By employing this optimum quantum state in the dark port, the quantum noise and optimum laser power reduce one order of magnitude relative to the conventional interferometers (Tofighi et al., 2010).

To minimize the effects of other noises, whole setup including optical elements and beam path are kept in ultra-high vacuum ($10^{-8} - 10^{-9}\ torr$) and the optical elements are suspended on top of the seismic isolation system. A highly stabilized laser and active control system for adjusting cavity length are employed in these devices. So the long baseline Laser interferometer GW detectors are high cost projects.

Fig. 24 shows another configuration for GW detection that uses optical fiber in the arms of Michelson interferometer. GW optical fiber interferometric detector is very small, cheap and simple to build and operate (Cahill, 2007; Sacharov, 2001; Cahill & Stokes, 2008).

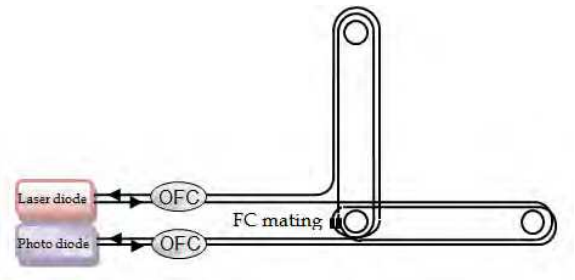

Fig. 24. A schematic of gravitational wave optical fiber interferometric detector.

7. Reference

Adams, M.J. (1981). *An Introduction to optical waveguides*. John Wiley & Sons Ltd. ISBN 0471279692

Agrawal, G. (Ed(4).). (2007). *Nonlinear fiber optics*. Academic Press, ISBN 0123695163, San Diego

Backman, A.B. (1989) *Journal of Lightwave Technology*, Vol. 7

Bahrampour, A.R. & Maasoumi, F. (2010). Resolution enhancement in long pulse OTDR for application in structural health monitoring. *Optical Fiber Technology*, Vol. 16, No. 4, pp. 240-249

Bahrampour, A.R.; Karimi, M.; Abolfazli Qamsari, M.J.; Rooholamini Nejad, H. & Keyvaninia, S. (2008). All optical set-reset flip-flop based on the passive microring resonator bistability. *Optics Communications*, Vol. 281, No. 20, pp. 5104-5113

Bahrampour, A.R.; Mohammadi Ali Mirzaee , S.; Farman ,F. & Zakeri, S.S. (2008). All optical flip flop composed of a single nonlinear passive microring coupled to two straight waveguides. *Optics Communications*, Vol. 282, No. 3, pp. 427-433

Bahrampour, A.R.; Zakeri, S.S.; Mohammadi Ali Mirzaee , S.; Ghaderi, z. & Farman ,F. (2008). All-optical set-reset flip-flop based on frequency bistability in semiconductor microring lasers. *Optics Communications*, Vol. 282, No. 12, pp. 2451-2456

Bahrampour, A. R. & Askari, A. A. (2006). Fourier-wavelet regularized deconvolution (ForWaRD) for lidar systems based on TEA CO_2 laser. Optics Communications, Vol. 257, No. 1, pp. 97-111.

Bahrampour, A. R.; Bathaee, M.; Tofighi, S.; Bahrampour, A.; Farman, F. & Vali, M. (2011).Polarization maintained optical fiber multi-intruder sensor. Submitted.

Bahrampour, A. R.; Moosavi, A.; Bahrampour, M. J. & Safaei, L. (2011). Spatial resolution enhancement in fiber Raman distributed temperature sensor by employing ForWaRD deconvolution algorithm. Optical Fiber Technology, Vol. 17, No. 2, pp. 128-134.

Barone, F.; Calloni, E.; De Rosa, R.; Di Fiore, L.; Fusco, F.; Milano, L. & Russo, G. (1994). Fringe-counting technique used to lock a suspended interferometer. *Applied Optics*, Vol. 33, No. 7, pp. 1194-119, ISSN 0003-6935

Bentley, S.J. & Boyd, R.W. (2004). Nonlinear optical lithography with ultrahigh sub-Rayleigh resolution, *OPTICS EXPRESS*, Vol. 12, No. 23, 5735-5740

Bohnert, K.; Gabus, P.; Nehring, J. & Brandle. H. (2002). Temperature and vibration insensitive fiber optic current sensor. *Journal of Lightwave Technology*, Vol. 20, No. 2, pp. 267-276

Boto, N.; Kok, P.; Abrams, D.S.; Braunstein, S.L.; Williams, C.P. & Dowling, J.P. (2000) Quantum interferometric optical lithography: exploiting entanglement to beat the diffraction limit. *Phys. Rev. Lett*, Vol. 85, No. 13, pp. 2733–2736

Bottacchi, S. (Ed(1).). (2008). *Noise and Signal Interference in Optical Fiber Transmission Systems: An Optimum Design Approach*. Wiley-Interscience, ISBN 0470060611

Brown, R.H. & Twiss, R.Q. (1956). Correlation between photons in two coherent beams of light, *Nature*, Vol. 177, No. 4497, pp. 27-29

Burns, W.K. (Ed(1).). (1993). *Optical Fiber Rotation Sensing*. Academic Press, ISBN 0121460754, San Diego

Cahill, R. T. (2007). Optical-Fiber Gravitational Wave Detector: Dynamical 3-Space Turbulence Detected. *PROGRESS IN PHYSICS*, Vol. 4, pp. 63-68, ISSN 1555-5534

Cahill, R.T. & Stokes, F. (2008). Correlated Detection of sub-mHz Gravitational Waves by Two Optical-Fiber Interferometers. *PROGRESS IN PHYSICS*, Vol. 2, pp. 103-110

Carrillo, A.; Gonzalez, E.; Rosas, A. & Marque, A.(2002). New distributed optical sensor for detection and localization of liquid leaks Part I. Experimental studies. *Sensors and Actuators A*, Vol. 99, pp. 229–235

Chelliah, P.; Murgesan, K.; Samvel, S.; Chelamchala, B.R.; Tammana, J.; Nagarajan, M. & Raj.B. (2010). Looped back fiber mode for reduction of false alarm in leak detection using distributed optical fiber sensor. *Applied Optics*, Vol. 49, No. 20, pp. 3869-3874

Chen, C.L.(2006). *Foundations for guided-wave optics*. John Wiley & Sons, ISBN 0471-75687-3

Choma, M.A.; Yang, C. & Izatt, J.A. (2003). Instantaneous quadrature low-coherence interferometry with 3×3 fiber-optic couplers. *Optics Letters*, Vol. 28, No. 22, pp. 2162-2164

Clark, T.R.; Carruthers, T. F.; Matthews, P. J. & I. N. D. III. (1999). Phase noise measurements of ultrastable 10GHz harmonically modelocked fiber laser. *Electron. Lett.*, Vol. 35, pp. 720–721

Cliche, J.F.; Painchaud, Y.; Latrasse, C.; Picard, M.J.; Alexandre, I.; Têtu, M. (2007). Ultra-Narrow Bragg Grating for Active Semiconductor Laser Linewidth Reduction through Electrical Feedback. *Proceeding in Bragg Gratings, Photosensitivity, and Poling in Glass Waveguides, OSA Technical Digest (CD) (Optical Society of America, 2007)*, paper BTuE2.

Crooker, C. M.; Garrett, S. L. (1987). Fringe rate demodulator for fiber optic interferometric sensors. Proceeding of Fiber optic and laser sensors, San Diego.

De Vos, K.; Debackere, P.; Claes, T.; Girones, J.; De Cort, W.; Schacht, E.; Baets, R. & Bienstman, P.(2009). Label-free Biosensors on Silicon-on-Insulator Optical Chips. *Proceedings of the SPIE*, Vol. 7397, pp. 739710-739710-8

Dianov, E.M.; Vasiliev, S.A.; Kurkov, A.S.; Medvedkov, O.I. & Protopopov, V.N. (1996). In-fiber Mach-Zehnder interferometer based on a pair of long-period gratings. *Proceedings of 22nd European Conference on Optical Communication - ECOC'96*, ISBN 82-423-0418-1, Oslo

Dong, X. & Tam, H.Y.(2007). Temperature-insensitive strain sensor with polarization-maintaining photonic crystal fiber based Sagnac interferometer. *APPLIED PHYSICS LETTERS,* Vol. 90, No. 15, pp. 151113

Dorrer, C.; Londero, P. & Walmsley, I.A. (2001). Homodyne detection in spectral phase interferometry for direct electric-field reconstruction. *Optics Letters*, Vol. 26, No. 19, pp. 1510-1512

Flourney, P.A.; McClure, R.W. & Wyntjes, G.(1972). White-light interferometric thickness gauge. *Appl. Opt*. Vol. 11, No. 9, pp. 1907-1915

Freitas, J.M.D.(2011). Recent developments in seismic seabed oil reservoir monitoring applications using fibre-optic sensing networks. *Measurement Science and Technology*, Vol. 22. No. 5, pp. 052001

Fu, H.Y.; Wu, C.; Tse, M.L.V.; Zhang, L.; Cheng, K.C.D.; Tam, H.Y.; Guan, B.O.; & Lu, C. (2010). High pressure sensor based on photonic crystal fiber for downhole application. Applied Optics, Vol. 49, No. 14, pp. 2639-2643

Gerry, C.C. & Knight, P.L. (2005). *Introductory quantum optics*. Cambridge University Press, ISBN 0-521-82035-9, New York

Glisic, B. & Inaudi. D.(2008). *Fibre Optic Methods for Structural Health Monitoring*. Wiley-Interscience, ISBN 0470061421

Gopel, W.; Jones, T.A.; Kleitz, M.; Lundstrom, I. Seiyama, T. (1991). *Chemical and biochemical sensors*. John Wiley and Sons, Vol. 2, ISBN 3527267697

Grattan, K.T.V. & Meggit, B. T. (Ed(1).). (1997). *optical fiber sensor technology: Devices and technology*. chapman & Hall, London

Grattan, K.T.V. & Meggit, B. T. (Ed(1).). (1999). *Optical Fiber Sensor Technology :Applications and Systems*, Kluwer Academic Publishers, ISBN 0-412-82570-8, United States

Harris, E.; Li, Yi.; Chen, L. & Bao, X. (2010). Fiber-optic Mach–Zehnder interferometer as a high-precision temperature sensor: effects of temperature fluctuations on surface biosensing. *Applied Optics*, Vol. 49, No. 29, pp. 5682-5685

Hassani, A. & Skorobogatiy, M. (2006). Design of the Microstructured Optical Fiber-based Surface Plasmon Resonance sensors with enhanced microfluidics. *OPTICS EXPRESS*, Vol. 14, No. 24, pp. 11616-11621

Haus, H.A.& Lai, Y.(1992). Theory of cascaded quarter wave shifted distributed feedback resonators. *IEEE J. Quantum Electron*. Vol. 28, No.1, pp. 205–213

Higuera, L.; Miguel, V. (2002). *Handbook of Optical Fibre Sensing Technology*. John Wiley & Sons, ISBN 0471820539, England

Hoeling, B.M.; Fernandez, A.D.; Haskell, R.C. & Petersen, D.C. (2001). Phase modulation at 125 kHz in a Michelson interferometer using an inexpensive piezoelectric stack driven at resonance. *Review of Scientific Instruments*, Vol. 72, No. 3, pp. 1630 – 1633, ISSN 0034-6748

Hong, C.K.; Ou, Z.Y. & Mandel, L. (1987). Measurement of subpicosecond time intervals between two photons by interference. *Phys. Rev. Lett*. Vol. 59, No. 18, 2044 2044–2046

Huang, H.C. (1984). *coupled mode theory as applied to microwave and optical transmission*, VNU Science Press, ISBN 90-6764-033-6, Netherlands

Jackson, D.A.; Kersey, A.D.; Corke, M. & Jones, J.D.C. (1982). Pseudo heterodyne detection scheme for optical interferometers. *Electronics Letters*, Vol. 18, No. 25, pp. 1081-1083

Jayanthkumar, A.; Gowri, N.M.; Venkateswararaju, R.; Nirmala, G.; Bellubbi, B.S. & Radhakrishna, T. (2006). Study of fiber optic sugar sensor. *PRAMANA journal of physics*, Vol. 67, No. 2, pp. 383-387

Jia, D.; Fang, N.; Wang, L. & Huang, Z. (2008). Distributed Fiber Optic In-Line Intrusion Sensor System. *Proceeding of Microwave Conference, 2008 China-Japan Joint,* pp. 608 – 611, ISBN 978-1-4244-3821-1

Juarez, J. C.; Maier, E. W.; Choi, K. N.& Taylor, H. F.(2005). Distributed fiber-optic intrusion sensor system. *Journal of Lightwave Technology,* Vol. 23, No. 6, pp. 2081 - 2087, ISSN: 0733-8724

Kashyap, R. (1999). *Fiber Bragg Gratings*. Academic Press, ISBN 0-12-400560-8, UK

Lin, W.W.; Chang, C.F.; Wu, C.W. & Chen, M.C. (2004). The Configuration Analysis of Fiber Optic Interferometer of Hydrophones. *Proceeding of OCEANS '04. MTTS/IEEE TECHNO-OCEAN '04*, Vol.2 , pp. 589 – 592, ISBN: 0-7803-8669-8

Linde, D.V. (1986). Characterization of the noise in continuously operating mode-locked lasers. *Appl. Phys. B*, vol. 39, No. 4, pp. 201–217

Manojlovi, L . (2010). A simple white-light fiber-optic interferometric sensing system for absolute position measurement. *Optics and Lasers in Engineering*, Vol. 48, No. 4, pp. 486–490

Mercado, J.T.; Khomenko, A.V. & Weidner, A.G. (2001). Precision and Sensitivity Optimization for White-Light Interferometric Fiber-Optic Sensors. *Journal of Lightwave Technology*, VOL. 19, NO. 1, pp. 70-74

Mishra, A. & Soni,A. (2011). Leakage Detection using Fibre Optics Distributed Temperature Sensing. *Proceedings of 6th Pipeline Technology Conference 2011*, Hannover, Germany

Okamoto, K. (Ed(2).). (2006). *Fundamentals of optical waveguides*. Academic Press, ISBN 0125250967, San Diego

Olindo, C.; Sagioro, M.A.; Monken, C.H. & Pádua, S. (2006). Hong-Ou-Mandel interferometer with cavities: Theory. *Physical Review A*, Vol. 73, No. 4, pp. 043806-043806.10 ISSN 1050-2947

Poli, F.; Cucinotta, A. & Selleri, S. (2007). Photonic Crystal Fibers Properties and Applications. Springer ISBN 978-1-4020-6325-1,Netherlands

Polygerinos, P.; Seneviratne, L.D. & Althoefer, K. (2011). Modeling of Light Intensity-Modulated Fiber-Optic Displacement Sensors. *IEEE TRANSACTIONS ON INSTRUMENTATION AND MEASUREMENT*, VOL. 60, NO. 4, pp. 1408-1415

Rao, Y.J. (1997). Fibre Bragg grating sensors. *Meas. Sci. Technol*, Vol. 8, pp. 355–375

Righini, G.; Tajani, A. & Cutolo, Antonello. (2009). *An Introduction to Optoelectronics Sensors*, World Scientific Publishing, ISBN 9812834125

Sacharov, V. K. (2001). Linear Relativistic Fiber-Optic Interferometer. *Laser Physics*, Vol. 11, No. 9, pp. 1014–1018

Sagnac, G. (1913). L'ether lumineux demontre par l'effet du vent relatif d'ether dans un interferometre en rotation uniforme. The demonstration of the luminiferous aether by an interferometer in uniform rotation. *C. R. Acad. Sci*, Vol. 157, pp. 708-710

Sanders, S.; Park, N.; Dawson, J.W. & Vahala, K.J. (1992). Reduction of the intensity noise from an erbium-doped fiber laser to the standard quantum limit by intracavity spectral filtering. *Appl. Phys. Lett*, Vol. 61, No. 16, pp. 1889-1891

Scully, M.O. & Zubairy. M.S. (Ed(3).). (2001). *Quantum Optics*. Cambridge University Press, ISBN 0521435951, United Kingdom

Shizhuo Yin, S.; Ruffin, P.B. & Yu, F.T.S. (Ed(2).). (2008). *Fiber Optic sensor*. CRC Press, ISBN 978-1-4200-5365-4

Snyder, A.W.; Love, J.(1983). *Optical waveguide theory* . Springer. ISBN 0412099500

Song, G.; Wang, X. & Fang, Z. (2001).White-light interferometer with high sensitivity and resolution using multi-mode fibers. *Optik*, Vol. 112, No. 6, pp. 245-249

Starodumov, A.N.; Zenteno, L.A. & De La Rosa, E.(1997). Fiber Sagnac interferometer temperature sensor. *Appl. Phys. Lett*., Vol. 70, No. 1, pp. 19-21

Strauss, C.E.M. (1994). Synthetic-array heterodyne detection: a single-element detector acts as an array. *Optics Letters*, Vol. 19, No. 20, pp. 1609-1611

Tofighi, S.; Bahrampour, A.R. & Shojaee, F. (2010). Optimum quantum state of light for gravitational-wave interferometry. *Optics Communications*, Vol. 283, No. 6, pp. 1012-1016.

Tsuchida, H. (1998). Correlation between amplitude and phase noise in a modelocked Cr : LiSAF laser. *Opt. Lett.*, Vol. 23, pp. 1686–1688

Tucker, R.S. & Baney, D.M. (2001). Optical noise figure: theory and measurements. *Proceedings of Optical Fiber Communication Conference and Exhibit, 2001. OFC* ,Vol. 4, ISBN 1-55752-655-9, Califomia

Tucker, R.S. & Baney, D.M. (2001). Optical Noise Figure: Theory and Measurements. *Proceedings of Optical Fiber Communication Conference and Exhibit, 2001. OFC 1*, ISBN: 1-55752-655-9

Vali, V. & Shorthill, R.W. (1976). Fiber ring interferometer. *Appl. Opt*, Vol. 15, No. 5, pp. 1099-1100

Villatoro, J.; Finazzi, V.; Badenes, G. & Pruneri, V.(2009). Highly Sensitive Sensors Based on Photonic Crystal Fiber Modal Interferometers. Journal of Sensors

Villatoro, J.; Kreuzer, M.P.; Jha, R.; Minkovich, V.P.; Finazzi, V.; Badenes, G. & Pruneri, V. (2009). Photonic crystal fiber interferometer for chemical vapor detection with high sensitivity.*Optics Express*, Vol. 17,No. 3, pp. 1447-1453

Villatoro, J.; Minkovich, V.P. & Hernández, D.M. (2006). Compact Modal Interferometer Built With Tapered Microstructured Optical Fiber. *IEEE PHOTONICS TECHNOLOGY LETTERS*, VOL. 18, NO. 11, pp. 1258-1260

Wang,C.; Trivedi, S.; Kutcher,S.; Rodriguez, P.; Jin,F.; Swaminathan, V. ; Nagaraj, S.; Quoraishee, S. & Prasad. N.S. (2011). Non-Contact Human Cardiac Activity Monitoring Using a High Sensitivity Pulsed Laser Vibrometer. *Proceedings of Conference on Lasers and Electro-Optics (CLEO)* , ISBN: 978-1-4577-1223-4, Baltimore

Weihs, G.; Reck, M.; Weinfurter, H. & Zeilinger, A. (1996). All-fiber three-path Mach–Zehnder interferometer. *OPTICS LETTERS*, Vol. 21, No. 4, pp. 302-304

Yuan, L. (1997). White-light interferometric fiber-optic strain sensor from three-peak-wavelength broadband LED source. *APPLIED OPTICS*, Vol. 36, No. 25 pp. 6246-6250

Yuan, L. (2002). Multiplexed, White-Light Interferometric Fiber-Optic Sensor Matrix with a Long-Cavity, Fabry-Perot Resonator. *Applied Optics*, Vol. 41, No. 22, pp. 4460-4466

Yuan, L.; Liu, Y. & Sun, W. (2005). Fiber optic Moiré interferometric profilometry. *Proceedings of SPIE*, Vol. 5633, ISBN 9780819455888

Interferometry - Research and Applications in Science and Technology

Edited by Dr Ivan Padron

ISBN 978-953-51-0403-2
Hard cover, 462 pages
Publisher InTech
Published online 21, March, 2012
Published in print edition March, 2012

This book provides the most recent studies on interferometry and its applications in science and technology. It is an outline of theoretical and experimental aspects of interferometry and their applications. The book is divided in two sections. The first one is an overview of different interferometry techniques and their general applications, while the second section is devoted to more specific interferometry applications comprising from interferometry for magnetic fusion plasmas to interferometry in wireless networks. The book is an excellent reference of current interferometry applications in science and technology. It offers the opportunity to increase our knowledge about interferometry and encourage researchers in development of new applications.

InTech Europe
University Campus STeP Ri
Slavka Krautzeka 83/A
51000 Rijeka, Croatia
Phone: +385 (51) 770 447
Fax: +385 (51) 686 166
www.intechopen.com

InTech China
Unit 405, Office Block, Hotel Equatorial Shanghai
No.65, Yan An Road (West), Shanghai, 200040, China
中国上海市延安西路65号上海国际贵都大饭店办公楼405单元
Phone: +86-21-62489820
Fax: +86-21-62489821